Beam shaping of edge-emitting diode lasers using a single double-axial hyperboloidal micro-lens

Zhen-Nan Tian,[3] Li-Jie Wang,[2] Qi-Dai Chen,[1,4] Tong Jiang,[1] Li Qin,[2] Li-Jun Wang,[2] and Hong-Bo Sun[1,5]

[1]*State Key Laboratory on Integrated Optoelectronics, College of Electronic Science and Engineering, Jilin University, 2699 Qianjin Street, Changchun 130012, China*

[2]*Changchun Institute of Optics, Fine Mechanics and Physics, Chinese Academy of Sciences, 16 Dongnanhu Road, Changchun 130033, China*

[3]*College of Physics, Jilin University, 199 Jiefang Road, Changchun 130023, China*

[4]*e-mail: chenqd@jlu.edu.cn*

[5]*e-mail: hbsun@jlu.edu.cn*

Received October 4, 2013; revised November 1, 2013; accepted November 12, 2013; posted November 12, 2013 (Doc. ID 198933); published December 11, 2013

We report an innovative approach for beam shaping of edge-emitting semiconductor diode lasers using a single double-axial hyperboloidal micro-lens fabricated with femtosecond laser direct writing technology. The two hyperboloids of different axial lengths focus the light from fast and slow axes to an identical focal spot. The divergence angles were shaped from 60° and 9° to 6.9 and 32.3 mrad, respectively, and the single-end fiber coupling efficiency is measured higher than 80%. The device is simple in fabrication, robust in structure, and easy for operation, by which multiple reflections and absorptions at interfaces are reduced, and assembly errors are minimized.

OCIS codes: (220.3630) Lenses; (120.1680) Collimation; (220.4000) Microstructure fabrication.
http://dx.doi.org/10.1364/OL.38.005414

Semiconductor diode lasers have been applied in broad industrial fields from fiber-optical communication to laser fabrication [1–3] due to their advantages of small size, easy integration, high efficiency, long lifetime, and relatively low cost [3,4]. Edge-emitting semiconductor diode lasers (EESDL) are particularly promising in laser material processing and laser fabrication because of their high output power and high reliability. While a major drawback that is hindering their current application is the poor output-beam quality [5–7], i.e., the large and asymmetric output-beam divergence angles, generally 30°–60° for fast axis and 10°–15° for slow axis directions. This is undesirable when high-quality laser processing and laser micro-nanofabrication are pursued, for which mode quality becomes an essential factor [8,9]. Over the past decades, many research efforts have been devoted to beam shaping of diode lasers, and various technologies have been proposed including a stepped reflecting mirror by Ehlers *et al.* [10], gradient index lens by Yamaguchi *et al.* [11], two reflective mirrors by Clarkson and Hanna [5], internal reflection prism by Wang *et al.* [12], diffractive optics by Skeren *et al.* [13], and refractive–diffractive hybrid lens by Pawlowski *et al.* [14]. Despite the fact that significant progress has been achieved because of the pioneering works, most of these technologies involve usage of a complicated set of optical components, for example, the combination of two orthogonal cylindrical lenses, each responsible for beam shaping along an axis. Assembling error and system instability is therefore inevitable, and the output energy is reduced due to multiple reflection, scattering and absorption at components surfaces and interfaces, and wavefront divisions degrades the beam quality. These remaining technical challenges call on simple, integrated, stable, and efficient optical shaping components.

We solve this problem in this Letter by a single double-axial hyperboloidal micro-lens, whose surface profile is defined by two hyperboloids. A hyperboloidal lens profile was adopted here because of its intrinsic capability to eliminate spherical aberration [15]. The axial length of each hyperboloid is customized according to individual diode lasers. Experimentally, the complicated lens structure was realized by femtosecond laser direct writing, a technology known for its unique high-precision three-dimensional (3D) prototyping capability [16–19].

The divergence angles of the output beam from an EESDL were different in the directions of vertical and parallel to junction plane [Fig. 1(a)], around 60° and 10°, and the associated directions are termed as fast axis and slow axis, respectively. This is easily manifested

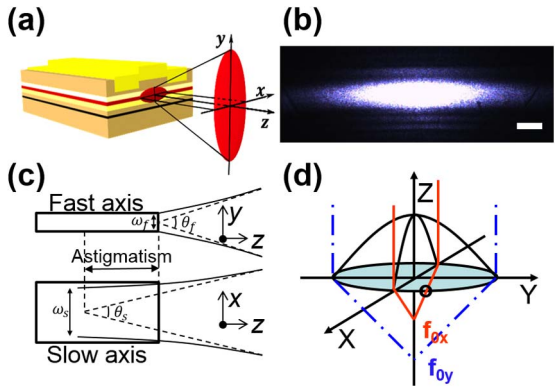

Fig. 1. Double-axial hyperboloidal micro-lens for beam shaping. (a) Schematic of EESDL and the single beam-shaping micro-lens. (b) Output beam spot from an 808 nm diode laser (scalebar 1 cm). (c) Schematic of divergence angles and beam waist in the fast axis and slow axis, respectively. (d) Schematic double-axial hyperboloidal micro-lens.

from the photograph of the light spot obtained 5 cm from the emitting surface of an 808 nm diode laser [Fig. 1(b)]. The divergence results from the rectangular side light emission window, which is defined by tens of nanometers of quantum well active layer (vertical direction) and several micrometers of light confined region width (lateral axis). This leads to different beam waist positions of fast axis and slow axis inside the laser cavity [Fig. 1(c)], i.e., intrinsic astigmatism exists in the output beam. In the fast axis direction, the output beam exits in single mode and the beam waist is positioned near the emitting surface. While in the slow axis direction, the output beam takes the form of multiple mode and the beam waist is far from the surface [Fig. 1(c)]. Since the difference of the focal lengths from the two axes is basically equal to the distance between the two beam-waist positions, we calculate the latter for proper lens design. Considering the relationship of the divergence angle and the beam waist, and following the propagation law of Gaussian beam, we have

$$\theta_0 = 2\frac{\lambda}{\pi\omega_0}, \tag{1}$$

$$\omega(z) = \sqrt{\omega_0^2 + \frac{z^2\lambda^2}{\pi^2\omega_0^2}}. \tag{2}$$

The inter-beam waist distance is calculated to be $\Delta z = 120$ μm with experimentally measured values of $\theta_0 = 60.2°$ and $\omega_z = 1.5$ μm for fast axis, $\theta_0 = 9.3°$ and $\omega_z = 10$ μm for slow axis, and $\lambda = 808$ nm. The focal lengths of the two hyperboloids are therefore set to f_{ox} (fast axis) and $f_{oy} = f_{ox} + 120$ μm. In order to determine the absolute value of f_{ox}, two factors have to be considered, the lens divergence capability and the spot size. Larger focal length benefits reduction of the beam divergence, while it demands larger distance from the emitting surface to the shaping lens and therefore a larger light spot size. For separated diode laser beam shaping, the light spot area is not limited, while for a diode laser array, the inter-diode laser distance restricts lenslets distance and spot size. Since the ultimate goal of our research is a micro-lens array for beam shaping of a diode laser array, the beam spot size has to be chosen smaller than the lenslet space, at a level of hundreds of micrometers. Experimentally it is chosen as $f_{ox} = 200$ μm and $f_{oy} = 320$ μm.

We fabricated the special 3D shaped lens using femtosecond laser-induced two-photon polymerization of photoresists, a technology that has been successfully employed in producing micromechanical and optical microstructures [20]. Femtosecond laser pulses of a wavelength of 800 nm with a pulse width of 120 fs, mode locked at 82 MHz (from Tsunami, Spectra-Physics), were focused by a high numerical aperture objective lens of NA = 1.4. The laser beam was scanned with a two-galvano-mirror set along the horizontal plane, and along the optical axis by a piezo stage, both with motion accuracy of 1 nm [21,22]. The photoresist samples were prepared by spin coating SU-8 films on a glass slide that was cleaned with acetone and absolute ethanol. The photoresist embedding the laser written structures was to be rinsed by the developer for 10 min so that the unpolymerized photoresist would be removed, leaving a solid skeleton.

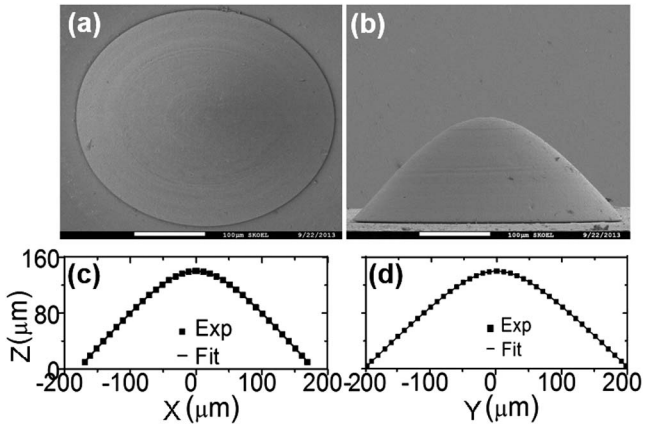

Fig. 2. Surface morphology and profile of double-axial hyperboloidal micro-lens. (a) and (b) SEM images of a lens, taken from top and side directions, respectively. (c) and (d) Surface profiles along the long and short axes taken by LSCM. Note the difference of the scale in the lateral axes.

The appearance of an experimentally produced double-axial hyperboloidal micro-lens was shown in Fig. 2. An elliptical cross section in the lateral direction is recognized from the top-view scanning electron microscopic (SEM, JSM-7500F, JEOL) image [Fig. 2(a)], showing the axial lengths of two hyperboloidal microlenes, 400 and 340 μm. The lens height that is commonly shared by the two hyperboloids is 139 μm [SEM side view, Fig. 2(b)]. In order to quantitatively examine the surface profile, a laser scanning confocal microscope (LSCM, OLS3000, EVC electronic) was utilized. The vertical cross section along the fast axis direction is shown as Fig. 2(c), while Fig. 2(d) is the cross-sectional profile along the slow axis direction. Judging from the above data extracted from the synthesized 3D digital images, the maximal deviation of the experimental structure from the theoretical design is less than 1%, if the deviation is defined as $(H_{\text{exp}} - H_{\text{des}})/H_{\text{des}}$, where H_{exp} and H_{des} denote experimentally attained and theoretically designed heights of an identical surface pixel of the lens. These results demonstrate that the digital lens model has been faithfully converted to matter structure by femtosecond laser direct writing.

The lens works by simultaneously reducing the beam divergence angles in both the fast and slow axial directions. Since the beam waists in these two directions are not spatially overlapped, but spaced on the optical axis normal to the emitting surface of an EESDL by a certain distance, two lenses are generally needed. Each is responsible for compensating the divergence in a direction. Here, the double-axial hyperboloidal micro-lens possesses two focal spots, which are able to be adjusted to overlap the two beam waists simultaneously. Therefore, beam shaping in two directions was fulfilled by a single lens. By fixing the lens to the EEDSL and aligning it, we reduced the 12 parameters (the conventional double cylindrical lens system) for fixing the relative positions of three 3D objects, here the EEDSL and two

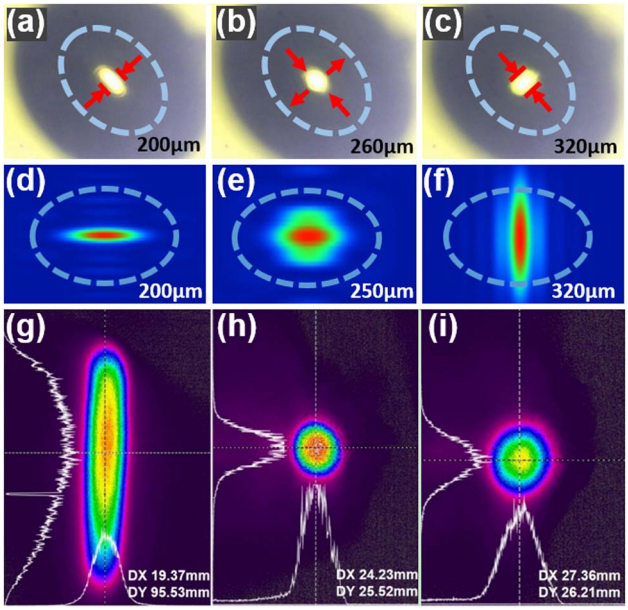

Fig. 3. Optical properties of a double-axial hyperboloidal micro-lens. (a)–(c) Optical photographs of light spots at different locations when the detector was drawn far from the emitting surface, (a) 200 μm, (b) 260 μm, and (c) 320 μm, respectively. (d)–(f) Ray tracing calculation of the focal spot shape by assuming an ideal plane wave incidence, indicating the capability of the shaping lens for correcting the divergences along the two individual directions. (g) Light output spots without the shaping lens, taken 5 cm away from the light emitting surface. (h) and (i), with the shaping lens, the beam was focused into near-round shape at the two focal spots. The photos were taken 15 cm and 25 cm away from the emitting surface.

lenses, by 50% since a single lens is adopted here. In detail, the lens was fixed on a turn table (accuracy 0.873 mrad) that was rotatable about the optical axis. Then, the turn table was fixed on a displacement platform (accuracy 2 μm). Finally, the lens gradually approached the emitting surface of the EESDL to determine the optimal position by monitoring the variation of light power behind the lens. Shown in Figs. 3(a)–3(c) are three light spot images that were taken at different positions along the optical axis as shown in Fig. 3. The distance for each adjacent spot is 60 μm. The detector was first placed near the lens surface and then drawn away along the optical axis. The light was first focused at the fast-axis direction [Fig. 3(a)], and then the slow-axis focal spot was met [Fig. 3(c)]. Figure 3(b) was taken between these two positions. The shaping affect has been confirmed by ray-tracing calculation [Figs. 3(d)–3(f)]. The dashed lines denote the shaping lens orientations. From Figs. 3(a)–3(c), the focal lengths of the two axes are calculated to be identical to the designed values, 200 and 320 μm, with a measurement error range of ±5%.

Since the output performance is device-dependent, the laser nanofabrication technology allows for personalized design and fabrication for individual shaping devices, for which its working parameter should be known beforehand [23,24]. The shape and energy distribution of light intensity were measured and then analyzed by an optical software, BeamGage. Figure 3(g) shows the original laser spot emitted from the EESDL, 5 cm from the emitting surface. The significant beam divergence as indicated by the oval light-spot shape is visible. The light-spot shape becomes almost a circle at positions of 15 [Fig. 3(h)] and 25 cm [Fig. 3(i)] away from the emitting surface because of the divergence compensation by the lens. The energy distribution is more concentrated than the original light spot. Using the far-field divergence angle formula

$$\theta_0 \approx 2\frac{w_1(z_1) - w_2(z_2)}{z_1 - z_2} = 2\frac{w_1 - w_2}{\Delta z}, \tag{3}$$

we obtained the divergence angles of the fast and slow axis of 6.9 and 32.3 mrad, respectively. These values are close to a theoretical prediction for transformation-limited beams. As a theoretical proof, we calculate the far-field distance (measured from the emitting surface)-dependent beam spot diameters and beam divergence angles in two directions [Fig. 4(a)]. At a position of 200 μm, spot sizes are 16.1 and 104.7 μm in slow and fast axis directions. Both are 2/3 smaller than the lens axis lengths, which ensures that almost all of the incident light passes through the shaping micro-lens. This implies that the length-focal-length design is appropriate for reducing energy waste and improvement of the shaping efficiency.

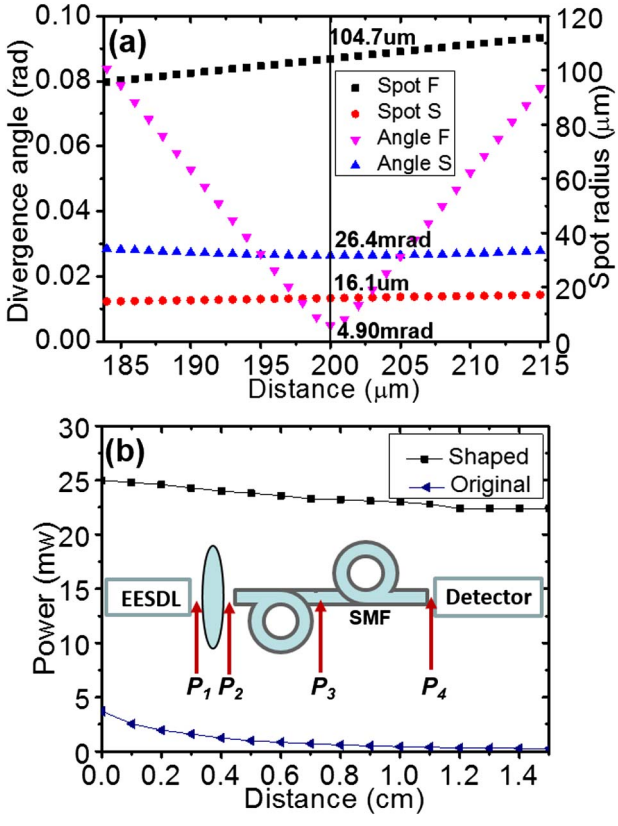

Fig. 4. Beam shaping performance for a customized micro-lens. (a) The predicted spot sizes from the EESDL (spot) and divergence angles of the shaped beam (angle) versus the distance from the emitting surface. Letters S and L denote the slow and fast axis, respectively. (b) Fiber coupling efficiency with (upper branch) and without (the lower branch) the shaping lens employed. The inset is the coupling optical configuration. The letters $P_1 - P_4$ are the laser power at different positions.

Fiber coupling of the shaped laser beam is one of the important steps toward high-power laser applications. To reach this end, we tested the fiber coupling efficiency. The diameters and refractive index of the core (cladding) are 10 μm (125 μm) and 1.448 (1.444), respectively, and NA = 0.107. In case of direct end-fire coupling without focusing, the power collected by the detector is always less than 5 mw and it rapidly decreases to nearly zero as expected [Fig. 4(b)]. In contrast, when the shaping lens is properly positioned between the laser and the fiber tip, the maximum single-end coupling efficiency reaches 89% and it maintains at a level of 80%, even if the space increases to centimeter order [Fig. 4(b)]. In this way, the Fresnel reflection has been considered. The reflectivity of the end facet is $R = 3.35\%$ according to the Fresnel reflection formula. For the efficiency calculation, the loss generated by the propagation of light in optical fiber was neglected. As shown in the inset of Fig. 4(b), the power incident on the fiber is P_2, and the power inside the fiber is P_3. P_3 is obtained according to the relation $P_4 = P_3 * (1 - R)$ since P_4 is directly read from the power meter (detector). The coupling efficiency is defined as P_3/P_2. The high-coupling efficiency means the laser light output from the shaping lens is well aligned and the divergence is sufficiently small.

In summary, we report in this Letter an innovative single-lens approach for laser beam shaping of EESDL. The greatly and asymmetrically divergent output beam from the fast and slow axis directions was focused into an identical focal spot because the double-axial hyperboloidal micro-lens works in two separated focal lengths. Such simple, robust, low-cost devices are feasibly produced and provided in a customized manner, showing its promising perspective in a high-power diode laser and diode laser array applications.

The authors acknowledge the financial support from the National Natural Science Foundation of China (NSFC) under Grant Nos. 90923037, 61137001, 61127010, and 61008035.

References

1. E. Murphy, Nat. Photonics **4**, 287 (2010).
2. D. Wu, L.-G. Niu, Q.-D. Chen, R. Wang, and H.-B. Sun, Opt. Lett. **33**, 2913 (2008).
3. F. M. Dickey, Opt. Photon. News **14**(4), 30 (2003).
4. S. T. Sanders, D. W. Mattison, L. Ma, J. B. Jeffries, and R. K. Hanson, Opt. Express **10**, 505 (2002).
5. W. A. Clarkson and D. C. Hanna, Opt. Lett. **21**, 375 (1996).
6. F. M. Dickey and D. L. Shealy, Proc. SPIE **5525**, 138 (2004).
7. J. R. Leger and W. C. Goltsos, IEEE J. Quantum Electron. **4**, 1008 (1992).
8. S. Shoji, S. Kawata, A. A. Sukhorukov, and Y. S. Kivshar, Opt. Lett. **27**, 185 (2002).
9. C. Roller, K. Namjou, J. D. Jeffers, M. Camp, A. Mock, P. J. McCann, and J. Grego, Appl. Opt. **41**, 6018 (2002).
10. B. Ehlers, K. Du, M. Baumann, H. G. Treusch, P. Loosen, and R. Poprawe, Proc. SPIE **3097**, 639 (1997).
11. S. Yamaguchi, T. Kobayashi, Y. Saito, and K. Chiba, Opt. Lett. **20**, 898 (1995).
12. Z.-J. Wang, A. Z. Gheen, and Y. Wang, "Optical coupling system for a high—power diode—pumped solid state laser," U.S. patent 6,377,410 B1 (April 23, 2002).
13. M. Skeren, I. Richter, and P. Fiala, Proc. SPIE **4095**, 154 (2000).
14. E. Pawlowski, M. Brinkmann, W. Beier, J. Luttmer, B. Wölfing, and P. Ebeling, "Refractive–diffractive hybrid lens, in particular for beam shaping of high power diode lasers," U.S. patent 7,345,828, B2 (March 18, 2008).
15. D. Wu, Q. D. Chen, L. G. Niu, J. Jiao, H. Xiao, J. F. Song, and H. B. Sun, IEEE Photon. Technol. Lett. **21**, 1535 (2009).
16. W. Xiong, Y.-S. Zhou, X.-N. He, Y. Gao, M. Mahjouri-Samani, L. Jiang, T. Baldacchini, and Y. F. Lu, Light Sci. Appl. **1**, e6 (2012).
17. K. Sasaki, M. Koshioka, H. Misawa, N. Kitamura, and H. Masubara, Opt. Lett. **16**, 1463 (1991).
18. A. Marcinkevicius, S. Juodkazis, M. Watanabe, M. Miwa, S. Matsuo, and H. Misawa, Opt. Lett. **26**, 277 (2001).
19. H.-B. Sun, S. Matsuo, and H. Misawa, Appl. Phys. Lett. **74**, 786 (1999).
20. Q.-D. Chen, X.-F. Lin, L.-G. Niu, D. Wu, W.-Q. Wang, and H.-B. Sun, Opt. Lett. **33**, 2559 (2008).
21. H.-B. Sun, T. Kawakami, Y. Xu, J.-Y. Ye, S. Matuso, H. Misawa, M. Miwa, and R. Kaneko, Opt. Lett. **25**, 1110 (2000).
22. K. Takada, D. Wu, Q.-D. Chen, S. Shoji, H. Hong, S. Kawata, and H.-B. Sun, Opt. Lett. **34**, 566 (2009).
23. C. Edwards, A. Arbabi, G. Popescu, and L. L. Goddard, Light Sci. Appl. **1**, e30 (2012).
24. D. Wu, S. Z. Wu, L. G. Niu, Q. D. Chen, R. Wang, J. F. Song, H. H. Fang, and H. B. Sun, Appl. Phys. Lett. **97**, 031109 (2010).